Hydrodynamic design of a bi-directional, rim-driven ducted thruster suitable for underwater vehicles

by

C. Pashias

S.R. Turnock

University of Southampton

Ship Science Report No.128

September 2003

Hydrodynamic design of a bi-directional, rim-driven ducted thruster suitable for underwater vehicles

by

C. Pashias

S.R. Turnock

University of Southampton

Ship Science Report No.128

September 2003

Table of Contents

Hydrodynamic design of a bi-directional, rim-driven ducted thruster suitable for underwater vehicles

by

C. Pashias

S.R. Turnock

University of Southampton

Ship Science Report No.128

September 2003

Summary

This report describes the hydrodynamic design process of an integrated thruster used for position control on a Remotely Operated Vehicle. The numerical analysis of the performance of the thruster is carried out using a lifting surface panel code with the Interaction Velocity Field method. The complete process is described from setting up the geometry model and validation, to selectign the optimised design.

The theory for the lifting surface panel method briefly described. The geometry of a marine propeller is described and the process of the mesh generation presented. The wake model is discussed in detail.

The numerical model was validated against the standard DTMB4119 open water propeller. The ducted model was validated with a standard Kaplan K470 series propeller in a Marin 37 duct and the experimental data from the two prototype bi-directional thrusters. The optimisation process of the thruster is presented and results presented.

Table of Contents

List of Figures

Nomenclature

U_∞	Free stream velocity	[m/s]
ω	Angular velocity	[rad/s]
R	Local radius	[m]
D	Propeller diameter	[m]
α	Angle of attack	[degrees]
α'	Modified angle of attack	[degrees]
C_P	Pressure coefficient $= 1 - \left(\frac{V_t}{V_R}\right)^2$	[-]
J	Advance ratio $= \frac{V}{nD}$	[-]
K_T	Thrust coefficient $= \frac{T}{\rho n^2 D^4}$	[-]
K_Q	Torque coefficient $= \frac{Q}{\rho n^2 D^5}$	[-]
n	Rotation speed	[Rev/s]
P	Section pitch	[m]
Q	Torque	[Nm]
T	Thrust	[N]
V	Advance velocity	[m/s]
V_R	$= \sqrt{V^2 + (2\pi nR)^2}$	[m/s]
V_t	Total edge velocity	[m/s]
η	Efficiency $= \frac{J}{2\pi}\frac{K_T}{K_Q}$	[-]

1 Introduction

The integrated thruster is an on-going project (Hughes 2000) developed for position control and propulsion of Remotely Operated Vehicles (ROV). The thruster is rim driven from a permanent magnet motor and offers considerable improvements (Abu-Shark 2003). Typically each ROV has six or eight thrusters: four for lateral and two or four for vertical position control. Most current thrusters have asymmetric propulsion characteristics, because of the use of off the shelf propellers coupled motor/shaft blockage effects.

A bi-directional thruster possesses an advantage over asymmetric thrusters. Bi-directionality simplifies the control problem since the same thrust is produced for the forward and reverse condition with the same rpm (Carlton 1994). The four quadrants become symmetric thus simplifying the control problem. The four quadrants being:

1. Forward thrust, forward motion
2. Forward thrust, reverse motion
3. Reverse thrust, reverse motion
4. Reverse thrust, forward motion

In addition an electric thruster has a lower number of parts, thus reducing maintenance costs. The electric thruster is also lighter which translates into more weight saving by reducing the syntactic foam required for buoyancy. Also no hydraulic power pack is required if an all-electric ROV is built, reducing weight even further. This gain in weight translates into more weight saving on the handling systems required on the ship.

The first phase of this project was to integrate the permanent magnet (PM) motor with the hydrodynamics of the thruster and to test the concept. Two prototype thrusters were built and tested. Phase one has been completed successfully.

Phase 2 of the model concentrated on improving the performance of the thruster by better motor-propeller matching and the use of a purpose designed bi-directional section. The thruster discussed in this report was optimised for use on a Hercules working class ROV, with a given motor specification.

The report is set out as follows: Section 2 describes the background theory for ducted propellers and the basic formulation of the numerical model used. Section 3 presents the propeller geometry and the discretisation of the model. The visualisation tools available are discussed in Section 4 and the validation of the numerical model with experimental results in Section 5. In Section 6 the optimisation process is described and results presented. Finally the conclusion is in Section 7. In Appendix A a more detailed description of generating marine propeller geometries from standard tables is given with an example. Appendix B gives a basic guide on how to use Propgen.

2 Theory

Ducted propellers have been widely used in applications where propeller diameter is limited. It is known that ducted propellers are more efficient than open water propellers under such operating conditions (McMahon 1994). The presence of the duct enables the propeller tip to sustain the pressure differential between the back and the face, thus generating more thrust to be developed with a smaller induced drag penalty. This is the reason why ducted propellers can have larger chords near the tip than conventional open water

propellers. Also the fact that the propeller is rim driven means that the larger tip chord loads do not have to be supported at the root which makes thinner root sections feasible.

There is a strong interaction between the duct and the rotor and because of the complex nature of the problem a non-viscous lifting surface panel method was used. Such methods can model complex problems quickly and have been used successfully in the past. The ease and time advantage over RANS codes (Turnock 2000) makes them ideal for optimisation studies.

The in house parallel lifting surface panel code, Palisupan (Turnock 1997), was originally developed to solve rudder-propeller interaction and follows the work of Morino (Morino 1974), Newman (Newman 1986) and Lee (Lee 1987). It involves a straightforward application of this method to model the interaction between a rotating propeller and duct.

Laplace's equation can be written as an integral over the bounding surface S of a source distribution per unit area s and a normal dipole distribution per unit area m distributed over the surface S. This can be expressed in terms of a surface integral as:

$$\phi = \int_{S_B} \int [\frac{1}{r}\sigma + \frac{\partial}{\partial n}(\frac{1}{r})\mu]dS + \int_{S_W} \int \frac{\partial}{\partial n}(\frac{1}{r})\mu dS \quad (1)$$

where S_B is the surface of the body and S_W a trailing wake sheet. In the expression r is the distance from the point for which the potential is being

determined to the integration point on the surface and $\partial/\partial n$ is a partial derivative in the direction normal to the local surface.

Equation (1) is discretised to give the following formulation for the potential at the centre of a given panel:

$$\phi_i = \frac{1}{2\pi}\sum_{j=1}^{N}\left((U_\infty \cdot n_j) S_{ij} - \phi_j D_{ij} \right) + \sum_{k=1}^{M} \Delta\phi_k W_{ik} \qquad (2)$$

For solving complex flows with multiple bodies the Interaction Velocity Field (IVF) method (Turnock 1994) is used, where the disturbance velocity field generated by a body is superimposed on the velocity field existing in the absence of the body.

For a duct/propeller problem an iterative process is employed as follows:

Step 1. The propeller is solved in the free stream velocity field.

Step 2. The propeller's disturbance velocity is applied to the free stream velocity field and the duct solved.

Step 3. The duct's disturbance velocity is applied to the free stream velocity field of the propeller and solved.

Step 4. Repeat steps 2 and 3 until the solution has converged.

Typically six iterations are required to converge within 0.5% of the total forces. The method effectively splits up the problem to smaller blocks reducing memory requirements and processing time. A typical run takes less

than 15min on a Pentium III 1Ghz for a 2000 panel problem using four rotational images (see section 3.3).

3 Mesh generation

In order to numerically model a propeller it must be discretised into a number of quadrilateral panels. The quality of the solution strongly depends on the quality of the mesh. Mesh generation is thus an important part of numerical modelling. Care must be taken to generate a correct mesh and the complex nature of propellers makes this a challenging task.

3.1 Propeller table

The complex shape of marine propellers is usually described by an offset table and 2-D section shapes. The table contains information about the pitch, chord, skew, thickness and rake at different radii along the blade. The propeller shape can be constructed from this information. Usually the information is non-dimensionalised with respect to the diameter of the propeller to enable easy scaling. Table 1 shows the propeller table for the Kaplan 4-70.

Ka-470 Propeller

r/R	c/D	Skew	Rake	P/D	t/c
0.2	0.231	0.0012	0	1	0.173
0.3	0.264	0.007	0	1.1	0.133
0.4	0.2935	0.004	0	1.15	0.102
0.5	0.32	0.002	0	1.2	0.077
0.6	0.345	0.003	0	1.25	0.055
0.7	0.365	0	0	1.3	0.038
0.8	0.379	0	0	1.3	0.024
0.9	0.388	0	0	1.3	0.016
1	0.389	0	0	1.3	0.013

Table 1- Propeller table for Kaplan470

3.2 Propeller geometry

In order to define the propeller blade geometry the following system is used, (Kerwin 1986). The blade is formed starting with a midchord line defined by the radial distribution of skew angle $\theta_m(r)$ and rake $x_m(r)$. By advancing a distance $\pm\frac{1}{2}\, c(r)$ along a helix of pitch angle $\phi_p(r)$, the blade leading edge and trailing edge are obtained. The surface formed by the helical lines is use as the reference upon which the sections can be built. These sections are defined in standard aerofoil terms by a chordwise distribution of camber $f(s)$ and thickness $t(s)$, where s is a curvilinear coordinate along the helix. A detailed description of the process is given in *Appendix B*.

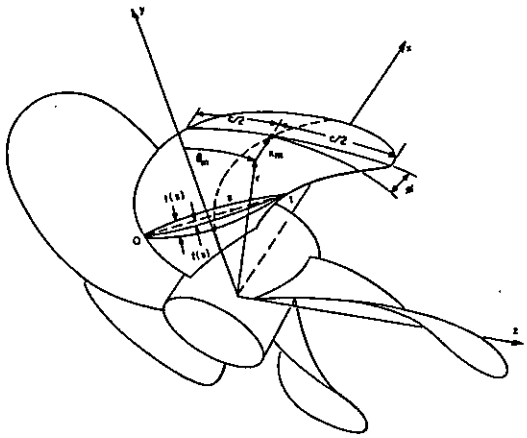

Figure 3.1 - Propeller geometry, Kerwin (1986)

3.3 Propgen

To generate a mesh for the propeller geometry a quick and simple method was required for a wide range of propellers. A program to discretise surfaces into to panels using transfinite interpolation (Hall 1973) was available, ***adaptflexi*** (Rycroft 1997). ***Adaptflexi*** requires an input of faces to generate the panelling. A program was required for the creation of these faces. A program called ***Propgen*** was developed for this purpose. ***Propgen*** creates a fleximesh file for use with ***adaptflexi***. It can handle most propeller geometries, including ducts. It can also generate an outer ring for use with tip driven propellers.

The generation of the propeller is simple. It requires an input of standard propeller data. The number of sections is set and the radii defined. The chord, thickness, skew, rake, pitch and the section shape are defined for each section. The propeller is then generated from the data. A duct, hub and ring can also be generated. The wake is also created using information from the file.

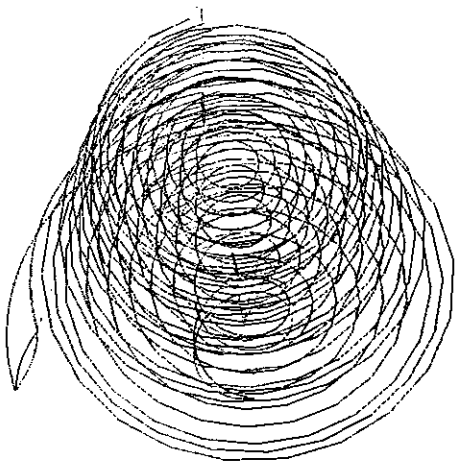

Figure 3.2 - Lines generated by Propgen to define a tip driven propeller with duct.

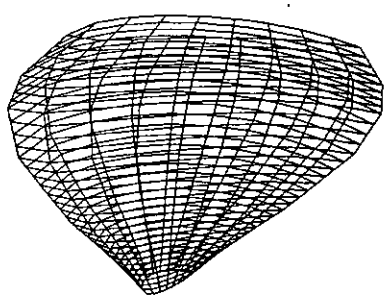

Figure 3.3 - Discretised propeller blade generated by adaptflexi from the lines in Figure

Only a segment of the complete geometry is generated. The model is then assumed to be rotationally symmetric since it's a steady case. The generated fleximesh file, which defines the surfaces, is then run through adaptflexi to generate the mesh for use with Palisupan. Palisupan then creates rotational images of the segment to model the complete thruster. This approach saves memory and computational effort (Pashias 2001). For unsteady problems a complete model can be generated within ***adaptflexi***.

If not enough edges are used to define surfaces with double curvatures it can lead to problems with the transfinite interpolation. Such a problem area is the duct. If the quarter section of the duct is defined with just the outer edges the resulting shape was not circular (Figure 3.4). To solve this problem the duct must be defined using ten sections, which gives more constraint points resulting in the correct circular shape.

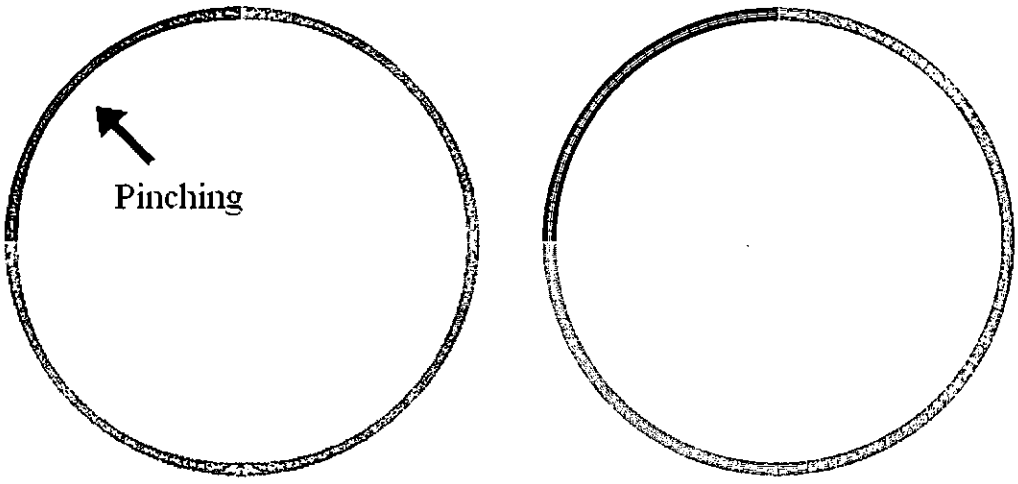

Figure 3.4 –(Left)- Non-circular duct created using only outer edges giving the wrong shape. The thinning of the duct is visible. (Right)-Circular duct defined using ten sections giving the correct shape

3.4 Wake model

In order for lift to be developed using a surface panel code a wakesheet must be defined in the wake of the lifting surface (Katz & Plotkin 2001). In the case of a foil operating in uniform flow the wake extends from the trailing edge of the foil downstream. The exact shape is not known in advance. It can be calculated using wake relaxation methods or wakesheet shedding techniques (Katz & Plotkin 2001). A close approximation is to extend the wake sheet linearly behind the lifting surface. This approximation gives acceptable results for most problems (Katz & Plotkin 2001).

For a propeller blade the wakesheet takes the form of helicoidal surface shed from the trailing edge of the blade downstream. The wake model is crucial for correct results. Wake relaxation methods have many numerical difficulties and are often unreliable. A difficult problem is due to the tip vortex causing the wake near the tip to roll back onto itself (Caponnetto 1997). This can be resolved by constraining the wake relaxation in one plane, but this defeats the point of the exercise. In addition, highly skewed panels can result which can cause numerical problems. Getting the relaxation to converge is another issue, even when damping is applied (Hughes 1998). A fixed wake model has been chosen because it is robust and quick. Fixed wake models have been used in the past giving as good results as shown in the 22nd ITTC Propulsion Committee workshop (Gindroz 1998).

The wake bisects the trailing edge of the blade and smoothly varies from that initial pitch to the final wake pitch. Since the experimental data from the two prototype thrusters were available, the final wake pitch was varied until there was good agreement.

The wake transitions from the initial to the final pitch in one propeller diameter. Instead of using a linear transition a 4th order polynomial was used which gives a smooth wakes shape. The wake pitch depends on the wake contraction and the polynomial is the same as the one used for the wake contraction (Hoshino 1991). A wake sensitivity study was carried out and a wake length of four diameters was found to be more than adequate with extra length only changing the thrust and torque by less than 1%.

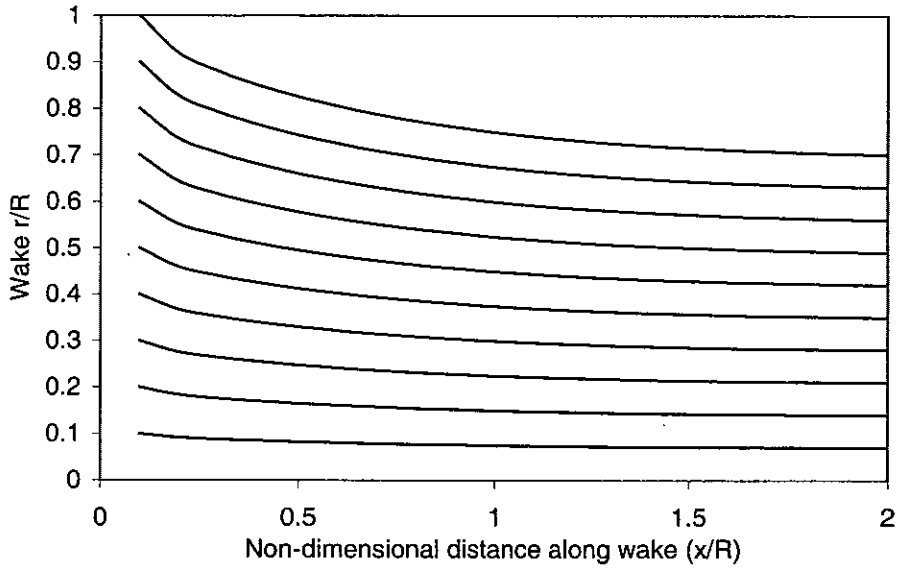

Figure 3.5 - Contraction shape for wake (Hoshino 1991)

As the flow is accelerated through the propeller it contracts downstream. Wake contraction increases with increased propeller loading and from experimental results is about 0.7D to 0.8D for most propellers (Hoshino1991, Pereira 2002). For heavily loaded propellers this is not negligible.

Since the variation in wake contraction appears to be small for normal propellers, the wake contraction has been accounted for by setting it to a fixed

value. A final wake contraction is assumed depending on the advance ratio. The wake contraction is set to this value for distances more than one diameter away from the blade. Between the blade and one diameter the wake contraction is modelled by a polynomial, which is based on experimental results (Hoshino 1991).

3.5 Hub considerations

The hub and ring have complex curvatures that need more than the outer edges to be defined correctly. So the hub and ring have to be split into longitudinal strips. On the hub and ring another problem that arises near the blade leading edge root. Because the discretisation of the surfaces results in panels that have sides parallel to the four edges defining the surface, if a continuous strip from the front to the back of the hub is used the panels cannot be created. To solve this problem the strips are split into smaller pieces. The first is divided by a line that bisects the angle between the hub edge and the blade nose root. The second is from the trailing end of one blade to the leading edge of the next and the last bisects the angle between the tail of the section and the hub edge.

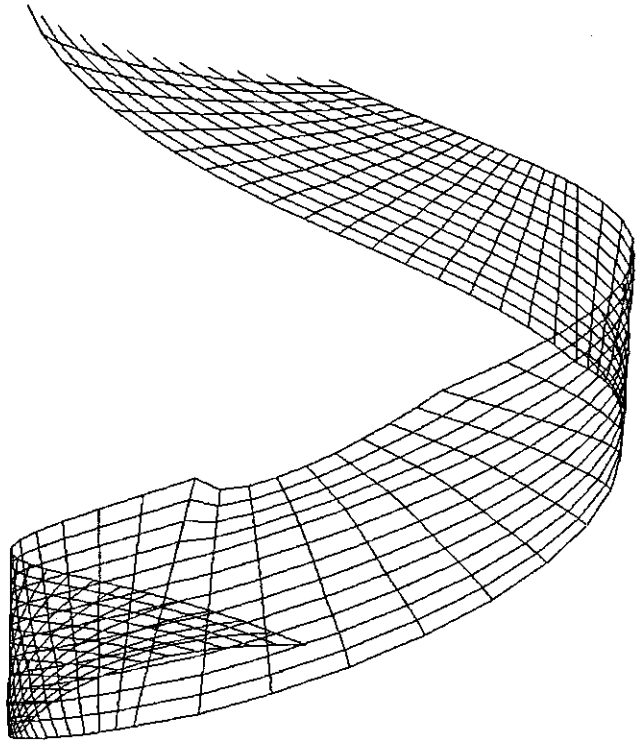

Figure 3.6 - Mesh for hub. The line at the section nose bisects the angle between the nose and the hub edge. The line from the trailing edge joins to the leading edge of the next blade.

When generating a mesh for a propeller with a hub care must be taken at the hub/wakesheet intersection. For propellers with normal sections the hub can be generated by a helix that has the pitch of the blade root. This is very similar to the wakesheet pitch, which bisects the trailing edge. However, for unusual section shapes, such as the bi-directional section shape the pitch of the section is substantially different and if the hub is generated as above the wakesheet intersects through the middle of the panels causing numerical problems on the hub. To solve this problem the pitch of the helixes generating the hub is the same as the wakesheet pitch. This ensures that the wakesheet and hub edge always match for all blade sections.

The end caps of the propeller were originally defined using radial sections. The requirement that the mesh is constituted from solely from square

panels meant that a small orifice at the nose was required. Studies with a sphere showed that this orifice had an effect on the flow, which although small was not negligible, especially on the boundary layer procedure, because a stagnation point is not present. To solve this a 'star' mesh was used on the nose, which eliminates the orifice. The mesh was validated for the case of a sphere and the results were in agreement. The stagnation point was captured better than the old mesh (Cp at nose of 1.0 compared to 0.99). In addition if panels are clustered near the orifice of the old mesh in an attempt to decrease the aspect ratio of the panels and use a small orifice, a small region of reversed flow into the orifice develops. The alternative to the 'star' mesh is placing a square patch on the nose with another four patches on the sides. This however cannot be used with the image model.

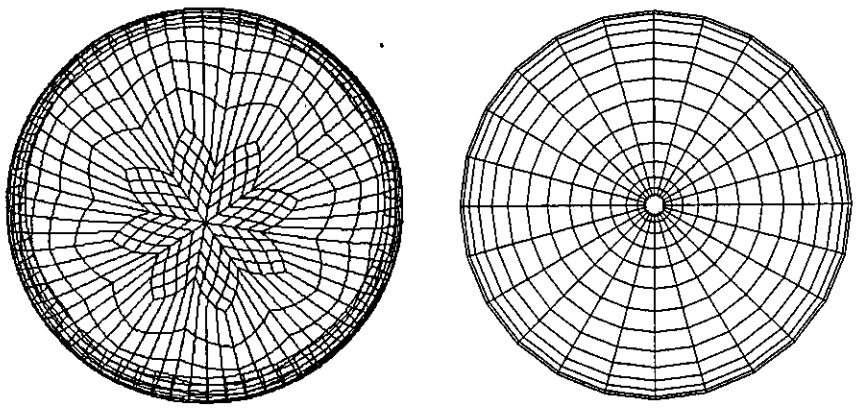

Figure 3.7 – End cap with 'star' mesh (left) without an orifice, giving improved results over the old mesh (right).

4 Visualisation

For three-dimensional geometries not having uniform or axisymmetrical flow, visualisation is important. The large amounts of data that numerical analysis techniques produce cannot be comprehended numerically for most cases. If symmetry exists then the data can be substantially reduced and standard graph techniques used. For more complex problems a better understanding of the flow is obtained if a three-dimensional colour map of a variable is plotted on the geometry. This visual presentation of the results enables the human mind to capture the complex nature of the flow more easily. Better understanding of the flow ultimately leads to improved designs. A visualisation tool was developed, ***PanVise***, for this purpose. It supports several file formats:

- Fleximesh - Geometry input file for adaptflexi and fleximesh mesh generators. Contains the face structure
- Pan files - Palisupan geometry files. Contain sections which define the geometry
- UNS files - Palisupan mesh file. Contains the panels of the geometry. Can be generated from adaptflexi
- AVS files - Standard output files from palisupan. Contains panels with local pressure coefficients and velocities.
- HFG files - Ship shape files.
- LFH files – Ship shape section file used for hydrostatic calculations.

Panvise can be used to view the face structure generated from ***Propgen***. The construction and end nodes can be viewed which makes finding mistakes easier. The mesh generated by ***adaptflexi*** can also be visualised and a colour map of aspect ratio can be plotted to view the mesh quality.

5 Validation

Before any numerical model can be used for optimisation purposes it must be validated for trustworthiness. This is preferably done against experimental data. In the absence of experimental data, other tried and tested numerical or theoretical methods can be used to validate against. If small changes to the geometry are made relative to the validated model then the numerical results can be assumed correct with a degree of certainty. To validate the mesh generation and numerical model, a standard propeller was selected. The DTMB4119 is standard open water three bladed propeller that has been used in the past for validation purposes and experimental data are readily available (Jessup 1998). This propeller has been used for the recent 22nd ITTC Propulsion Committee workshop (Gindroz 1998).

For the DTMB4119 a panel sensitivity study was carried out and 23 panels were used for the blade in the spanwise direction and 20 in the chordwise direction giving a total of 460 panels on the blade with an additional 288 on the hub and 5920 wake panels.

Different wake parameters have been investigated to find their influence on the results. Wake contraction and initial pitch have both been studied.

The initial pitch of the wake has been set to three different values: the local section pitch, the pitch of the bisector of the trailing edge and the pitch of the back face on the trailing edge. The influence has been found to be small giving a change in K_T of 1% and K_Q 0.2% from one extreme to the other. The wake geometry used has the initial pitch set to bisect the trailing edge.

The effect of wake contraction was found to have less than one per cent influence on the K_T and K_Q. For advance ratios close to one the effect was negligible whereas for smaller advance ratios there was a one per cent increase in K_T and K_Q rising with decreasing advance ratio as expected. As the influence was relatively small the wake contraction was not modelled in subsequent calculations.

The pressure distribution for an advance ratio of 0.833 was compared to the experimental data at r/R of 0.3, 0.7 and 0.9. The results were in good agreement with the experimental results and other panel code calculations. The pressures for the 0.9 radius are slightly over predicted, which was the norm for other codes (Hoshino 1998). In addition the K_T, K_Q for a range of J was compared, giving good agreement with the experimental data.

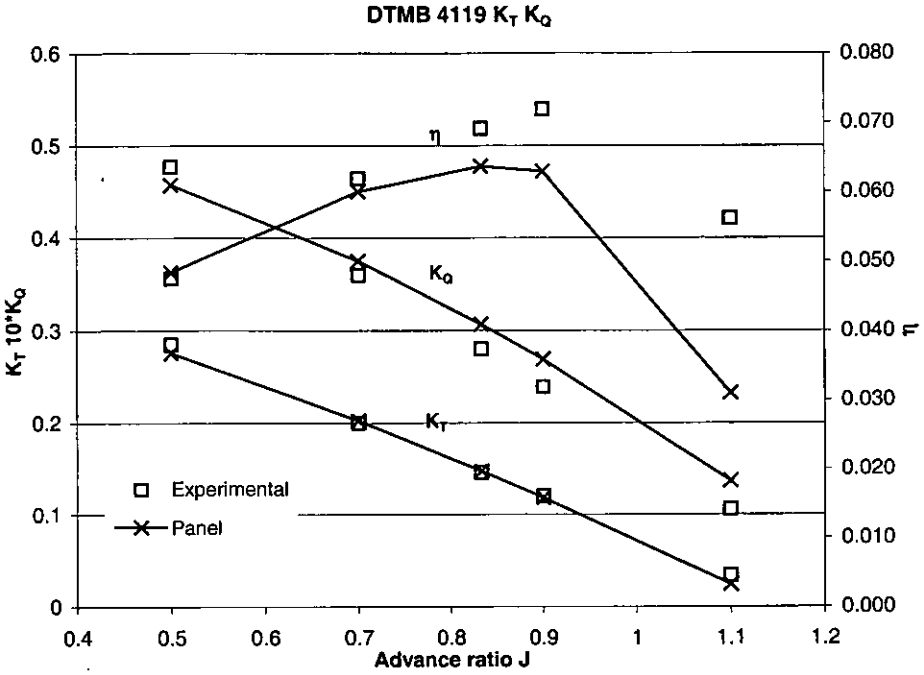

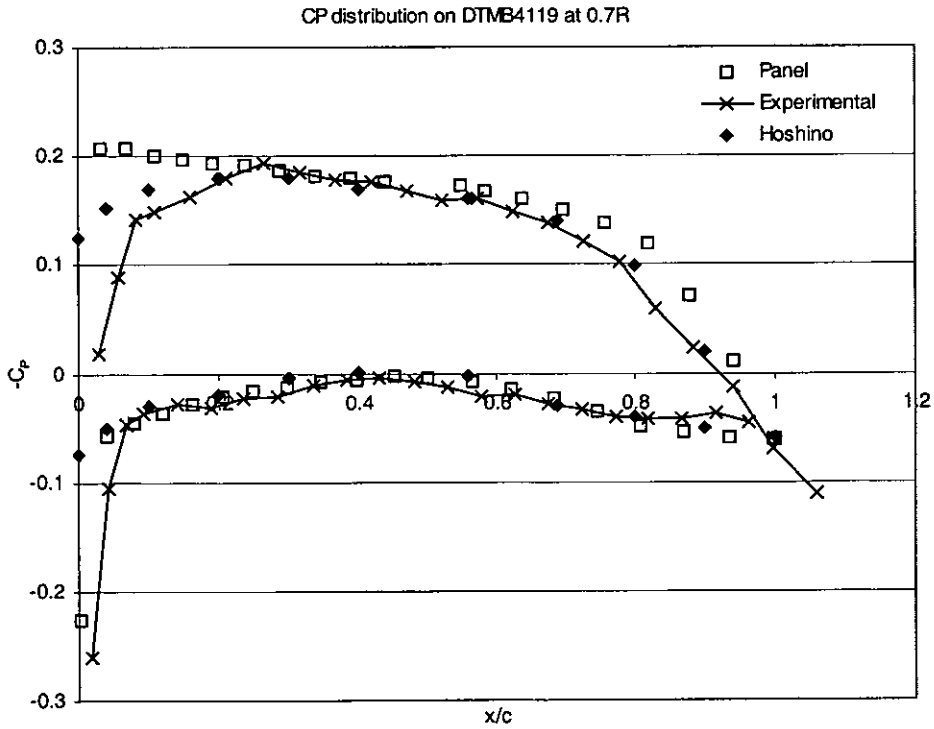

Figure 5.1 - Validation data for the DTMB4119

The numerical model of the duct and propeller was validated using experimental data from the two prototype thrusters. The thrusters were tested with different propeller/duct combinations and had symmetrical ducts and propellers with a P/D of 1.4 and 1.0. The thrusters were tested in a towing tank at different advance speeds and rpm. The thrust was measured using a dynamometer and the torque calculated from the input power. Losses for the wiring and bearings were deducted from the measured input power and the torque calculated. The depth restriction in the tank means that the thruster was operating near the free surface, which makes cavitation a possibility especially at the highly loaded cases. A graph of K_T and K_Q against rpm is shown in Figure 5.2. From the figure we can see that KT is fairly constant over the rpm range. However the KQ decreases with increasing rpm. This could be due to cavitation effects or viscous effects which do not scale proportionally with rpm.

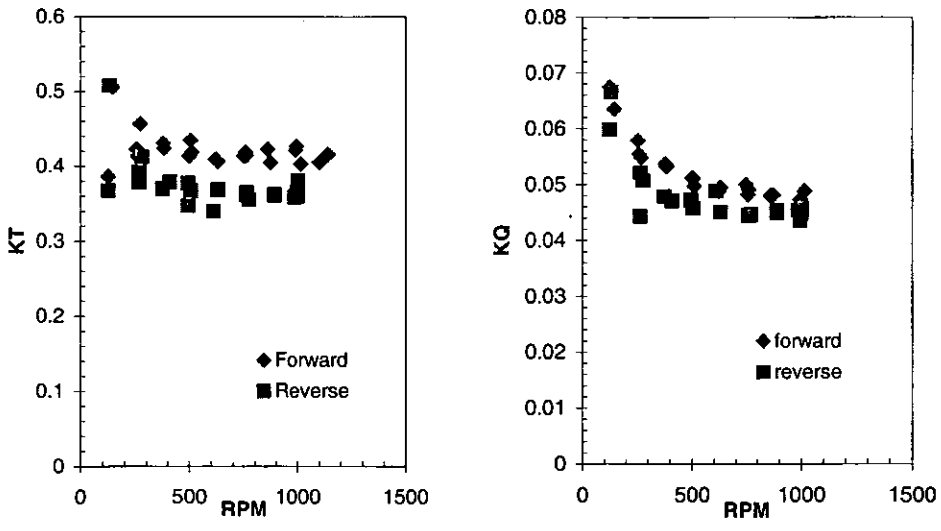

Figure 5.2 - KT and KQ vs RPM

A gap of 1% of the overall propeller diameter was left between the inner surface of the duct and the blade tip to eliminate the high C_P caused by the proximity of the blade tip to shielded panels on the duct. A study was carried out to find the effect of this gap on the results. The thrust was non-dimensionalised with respect to area and radial speed and plotted against the gap size. From the graph we can see that there is a rapid change near the 0.5% gap.

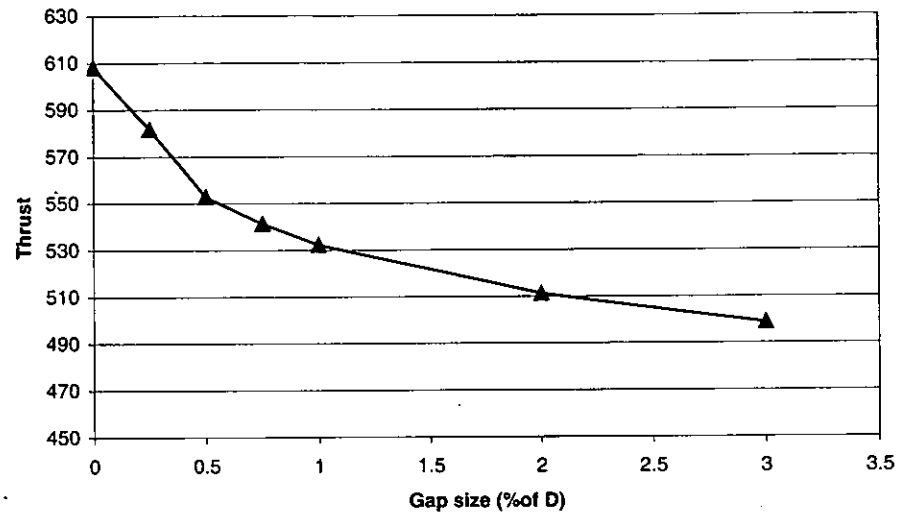

Figure 5.3 – Influence of gap size on solution

The numerical results were in relatively good agreement with experimental data. The slope of the K_T and K_Q curves do not match exactly with the experimental results. This is due to a number of reasons. The duct imposes a velocity and hence modifying the operating condition of the propeller. Since no form of wake relaxation was used this was not taken into account. Also ensuring the correct wake shape for heavily loaded propellers is difficult (Takinaci 2001). Another effect not taken into account is that the propeller

contraction also affects the duct wake, which will again alter the thrust of the duct.

In addition in this model no viscous interaction effects are included and for simplicity the six stators are neglected. However, as shown previously (Hughes 2000, Hughes 2001) the relative performance changes are captured well.

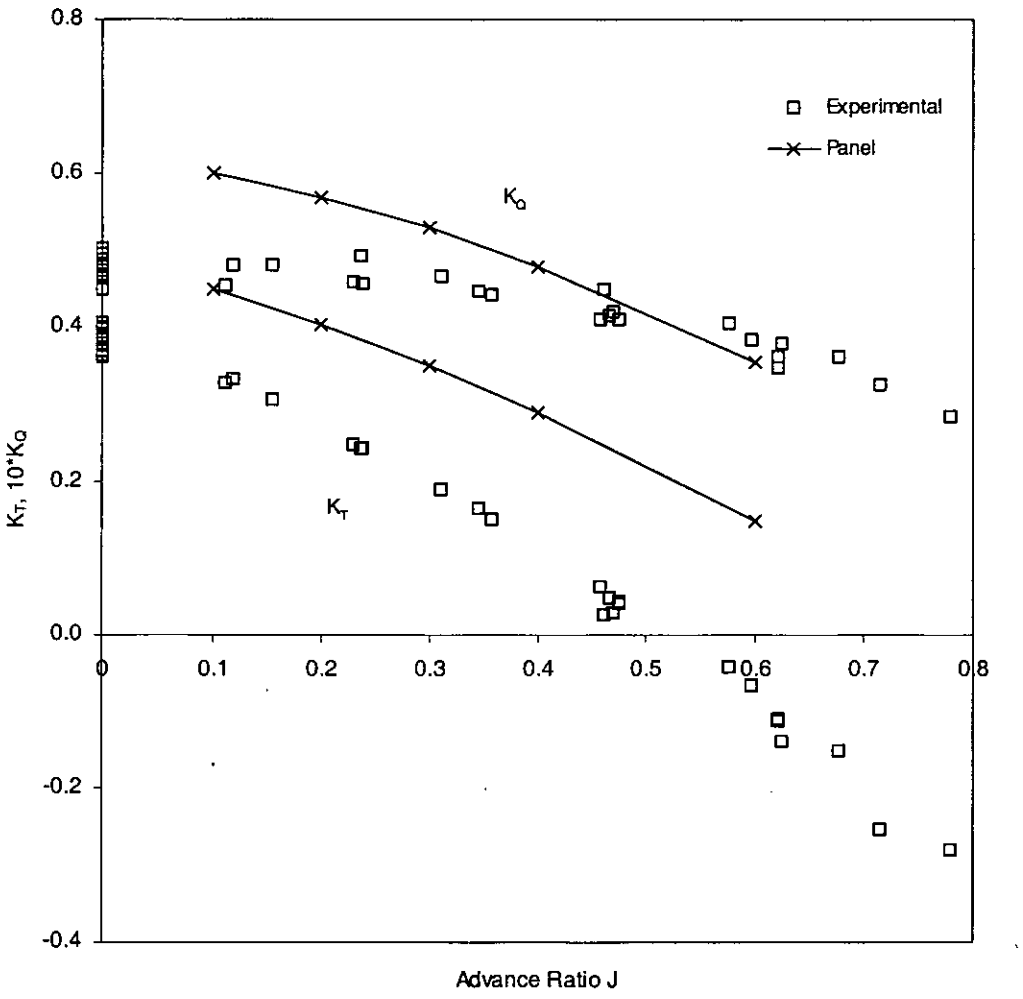

Figure 5.4 - Prototype K_T K_Q

6 Optimisation

6.1 Bi-directional propeller section

In order for the thruster to have identical performance forward and reverse. the foil section used has to have bi-directional characteristics. Such a section has to be rotationally symmetric. Bi-directional sections are not readily available. A new section was developed using a two-dimensional panel code, X-Foil (Drela 1989).

A starting point for the section was not available and a thorough investigation had to be carried out. An automated method for defining possible candidate sections was developed to speed up the optimisation process. A quintic polynomial was used to define the camber line, which was rotationally symmetric. A leading and trailing edge circle and two cubic splines were used to define the thickness distribution. The section shape was the created by adding the thickness to the camber line (Figure 6.1). The parameters controlling the camber and thickness were varied over a specified range and a series of bi-directional sections was produced. The sections were then analysed and refinements made to possible candidates. Over 10,000 sections were automatically created and tested (Ellsmore 2002).

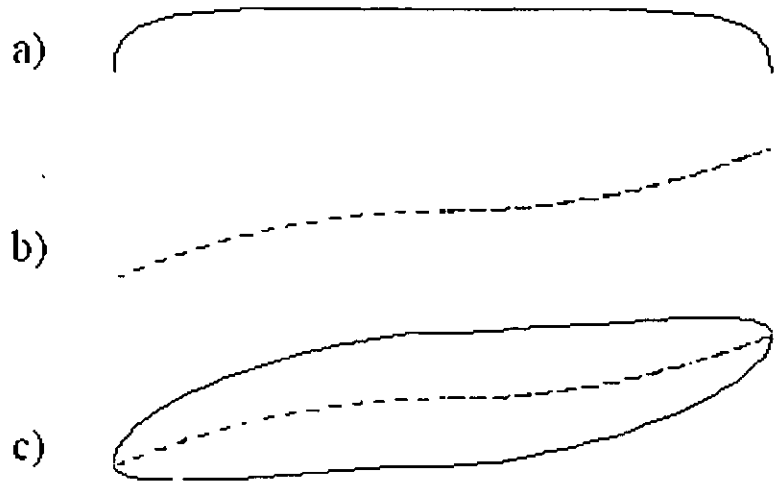

Figure 6.1 - Thickness distribution (a) is added to the camber (b) to generate a symmetrical section (c)

6.2 Duct

Standard asymmetric ducts such as the Marin37 can produce a substantial proportion of the thrust. This thrust is produced by the asymmetry in the shape of the duct. The slope in the ducts profile contracting downstream causes an increase in the velocity inside the duct compared to the free stream velocity. This increase in velocity results in a low pressure on the inner surface, which produces a forward thrust due to the slope of the duct's inner surface.

For symmetrical ducts the constraints means that the thrust generated by the duct is substantially less. The inner surface must be flat and any pressure difference due to highly curved sections does not result in thrust. In fact the increase in velocity due to the curved inner surface results in an effective increase in the advance ratio of the propeller decreasing thrust. The final design has relatively flat inner surface to minimise velocity in the duct.

Separation is also an issue at the trailing edge and leading edge. Sharp ends might eliminate separation at the trailing edge but when the thruster is operating at a yaw angle it will lead to separation at the leading edge. A compromise must be made between the two.

The influence of duct length was investigated at different speeds. The results show a variation of optimum duct length with speed (Pashias 2003). The optimum duct length increases with advance ratio. Since the thruster will be used for position control and will mainly operate at low speeds a short duct length was chosen. A compact design also has practical advantages when mounting on the ROV.

The hub must have minimum drag and provide uniform flow into the propeller. It also must house the shaft bearings. The hub length could not exceed the duct length for practical reasons.

6.3 Matching the propeller with the motor

The performance of the propeller/motor combination must be analysed rather than the individual components. An efficient propeller might not operate at the motor's optimum point resulting in a lower efficiency. Also the application of the propulsion unit must be considered. If for example, the thruster is for an Autonomous Underwater Vehicle then it is likely that maximum efficiency is required to keep the power requirements down and maximise range. On the other hand if it is installed on a Remotely Operated Vehicle with an umbilical cord supplying power from the mother ship then the design could be optimised to give maximum thrust irrespective of power consumption.

There are many parameters that can influence the performance characteristics of a propeller. Given diameter constraints the two main factors are blade area ratio (BAR), pitch and their distribution. BAR is usually determined by cavitation criteria for vessels operating near a free surface. The pitch is mainly dependant on the advance ratio of the propeller. The higher the advance ratio the higher the optimum pitch.

A good starting point for any propeller optimisation process is a standard series propeller. A considerable amount of work has gone in the designing of standard series propellers and they have optimum chord distributions and pitch variation for most applications.

The optimisation process varies depending on the limitation imposed upon the design. For vessels operating near the free surface, diameter and cavitation limits usually apply. These restrictions give a design starting point. With the diameter and BAR (selected to avoid cavitation) known, the pitch and chord distribution need to be optimised. In addition an rpm restriction frequently applies which means that the section pitch can be calculated from the ideal incidence angle of the section. For the thruster the only restriction is the diameter. The BAR, rpm, P/D are all variables.

As the BAR decreases the efficiency of the propeller increases due to a reduction in frictional resistance. This tendency holds up to the point where the section thickness has to be increased due to strength requirements causing an increase in form drag.

The optimum pitch for a given advance ratio does not change drastically with BAR. A study can be carried out with different pitch ratio to determine the optimum.

The optimum chord and pitch distribution varies with the propeller type. The best chord distribution gives optimum loading along the blade, and thus minimum induced drag. Then depending on the inflow velocity distribution, if the propeller is operating in a wake, alter the pitch distribution such that the blade sections all operate at the ideal angle of attack.

For ducted propellers the optimum chord distribution is different than open water propellers. The blockage effect of the duct allows larger chords to be used at the tip. To find the optimum pitch distribution of a ducted propeller operating in open water the velocity profile induced by the duct on its own can

be used to calculate the change in the hydrodynamic pitch. Then this can be superimposed on the overall pitch.

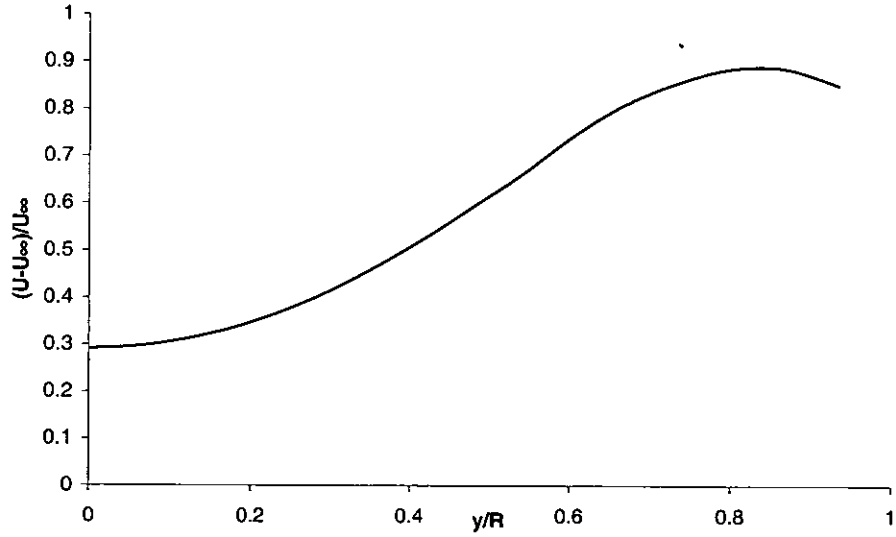

Figure 6.2 – Velocity Profile in duct of diameter 0.3m at a free stream velocity of 0.6m/s

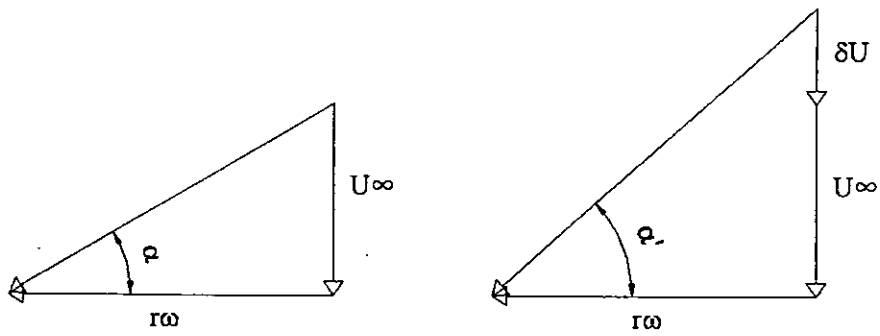

Figure 6.3 – Velocity triangle for propeller section

$$\tan\alpha = \frac{U_\infty}{r\omega}$$
$$\tan\alpha' = \frac{U_\infty + \delta U}{r\omega} \qquad (0.3)$$
$$d\alpha = \tan^{-1}\left(\frac{U_\infty + \delta U}{r\omega}\right) - \tan^{-1}\left(\frac{U_\infty}{r\omega}\right)$$
$$dP = 2\pi r.d\alpha$$

From equation (0.3) we can see that at high rpm relative to the free stream disturbance the change in hydrodynamic pitch is negligible. Also for very slow rpm the change is also negligible.

$$\lim_{\omega\to\infty} d\alpha \to 0$$
$$\lim_{\omega\to 0} \tan\alpha \to \pi/2 \qquad (0.4)$$
$$\therefore \lim_{\omega\to 0} d\alpha \to 0$$

For a propeller operating in the duct shown in Figure 6.2 at 1200rpm the change in pitch is shown below.

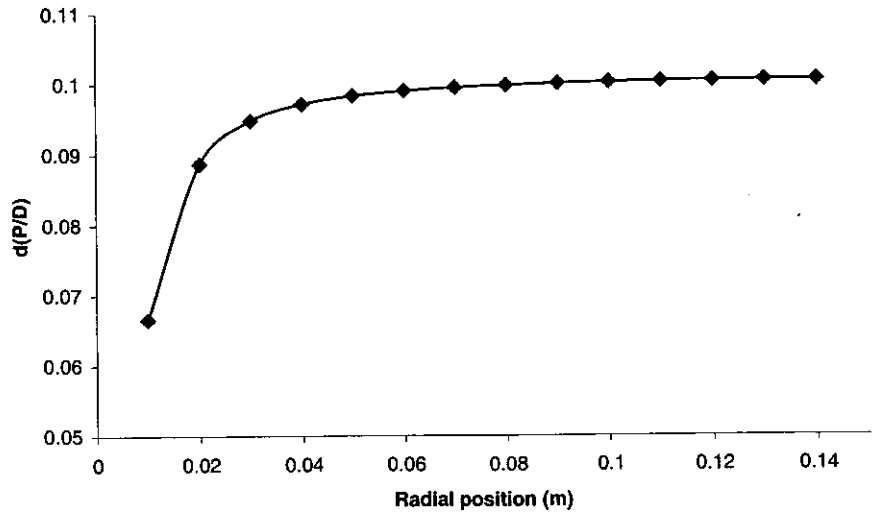

Figure 6.4 – Change in P/D due to the duct

It is vital that the thruster is considered as one unit when optimising. There is no point designing an efficient propeller if the motor cannot operate at those conditions or is relatively inefficient.

The BAR and chord distribution of the prototype thruster were selected as a starting point. This is very similar to the Kaplan 470 standard series propeller. The pitch distribution was calculated as described above for the selected duct.

The operating envelope is defined by the following restrictions and characteristics. The motor torque curve, which is a characteristic of the motor design. The max torque limit, which depends on the current the motor can absorb before it overheats. It is dependant on the cooling and motor design. The available power from the supply which has a limited capacity. The operating envelope is shown on (Figure 6.5)

The P/D of the propeller was varied systematically to find the optimum pitch ratio. At each P/D the rpm of the propeller was varied such that the torque available from the motor was absorbed. This gives a true indication of the performance of the thruster, rather than comparing the different propellers at the same rpm. From (Figure 6.5) we can see that at high rpm there is less torque produced by the motor and the lower pitch propellers even though more efficient hydrodynamically do not produce much thrust since the power absorbed is low. At lower rpm the motor develops more torque and the propeller absorbs more power albeit at lower rpm.

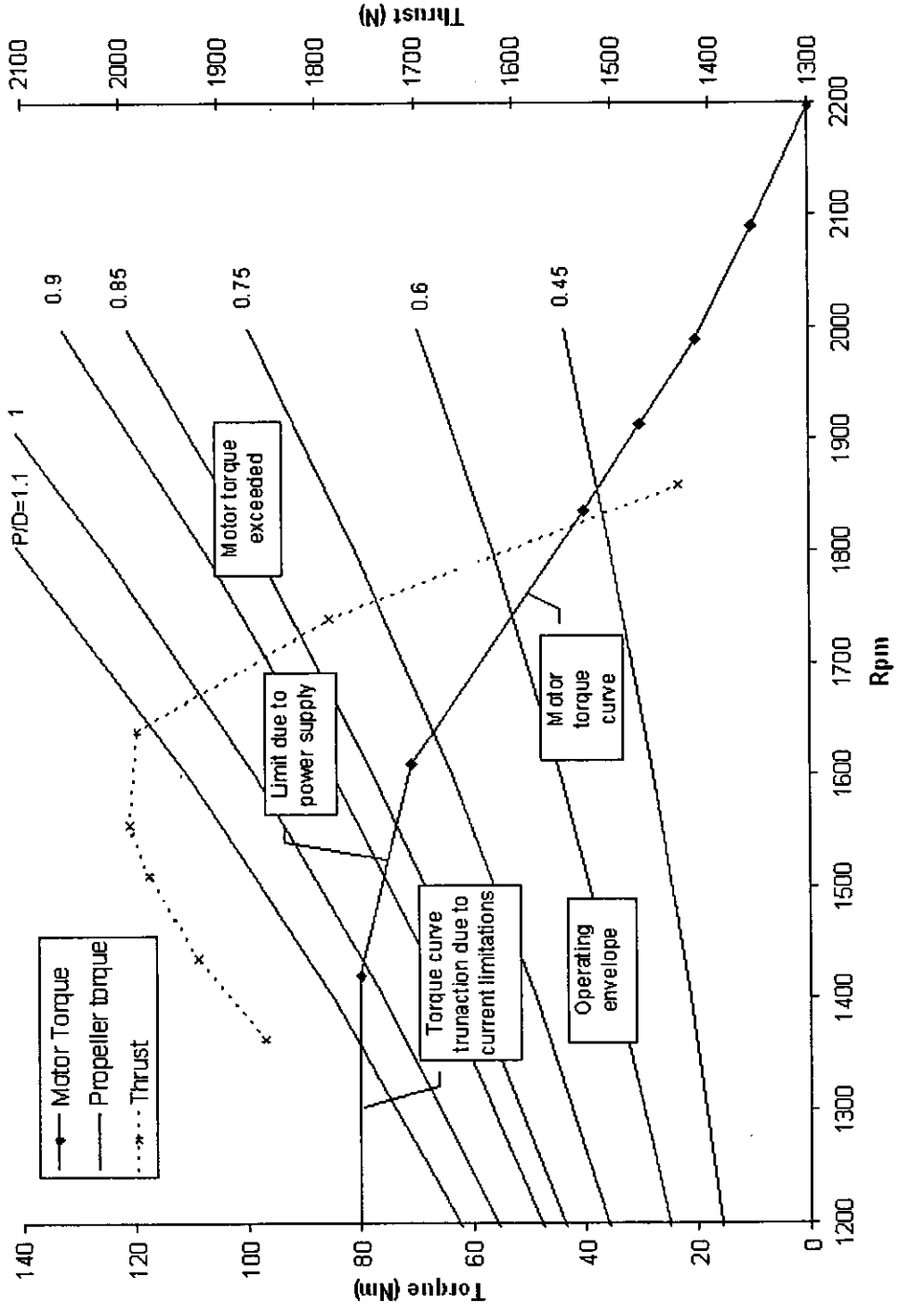

Figure 6.5 – Torque operating envelope with different P/D propeller curves shown. The operating condition is where the motor and propeller curves intersect

7 Conclusion

The complete process of the optimisation of an integrated thruster has been presented in detail. The process was described from the presentation of the problem to mesh generation, validation and optimisation. A mesh tool specific for marine propellers was developed. This enables meshes to be quickly generated from standard propeller tables and section offsets. The created mesh is suitable for the majority of marine propellers.

The numerical model presented here has a low computational cost which makes it ideal for optimisation studies. The relative performances are captured well and design optimisation is possible with such a method. The integrated thruster optimisation has been presented and the constraints discussed.

Computational Fluid Dynamics can be used for many applications but care must be taken to validate the models used and always condiser the limitations of the method.

8 References

CAPONNETTO M, "The aerodynamic interference between two boats sailing close-hauled." Int. Shipbuild. Progr., 44, no 439: 241-256, 1997

CARLTON J, "Marine Propellers and Propulsion", Butterworth Heinemann, 1994

DRELA M, "XFOIL: An Analysis and Design System for Low Reynolds Number Airfoils." Conference on Low Reynolds Number Airfoil Aerodynamics, University of Notre Dame, June 1989

ELLSMORE P, "Optimisation of a bi-directional section." Part III individual project, University of Southampton, 2002

GINDROZ B, HOSHINO T and PYLKKANEN JV editors, "Propeller RANS/Panel Method Workshop Proceedings." 22nd ITTC Propulsion Committee, Grenoble, 1998

HALL CA, "Construction of curvilinear co-ordinate systems and applications to mesh generation." International Journal for Numerical Methods in Engineering, 7:461-477, 1973.

HOSHINO T, "Numerical and experimental analysis of propeller wake by using a surface panel method and a 3-component LDV." 18th Symposium on Naval Hydrodynamics, 1991

HOSHINO T, "Comparative calculations of propeller performance in steady and unsteady flow using a surface panel method." 22nd ITTC Propulsion Committee, Propeller RANS/Panel Method Workshop, Grenoble, France, April 1998

HUGHES AW, TURNOCK SR and ABU-SHARKH SM, "CFD modelling of a novel electromagnetic tip driven thruster for underwater vehicles", ISOPE 2000, Seattle, June 2000.

HUGHES AW, "Investigation of Tip-Driven Thruster and Waterjet Propulsion Systems." PhD thesis, University of Southampton, 2001

HUGHES MJ and MASKEW B, "Calculations for the DTMB4119 and DTMB4679 propellers and a highly skewed propeller for the Sein-Maru using

the VSAERO/PROFAN and USAERO codes." 22nd ITTC Propulsion Committee, Propeller RANS/Panel Method Workshop, Grenoble, France, April 1998.

HUGHES AW, ABU-SHARKH S and TURNOCK SR, "Design and testing of a novel electromagnetic tip-driven thruster." The Proceedings of the 10th International Offshore and Polar Engineering Conference, Seattle, USA, pp.299-303, June 2000

JESSUP S, "Experimental data for RANS calculations and comparisons (DTMB4119)." 22nd ITTC Propulsion Committee, Propeller RANS/Panel Method Workshop, Grenoble, France, April 1998

KATZ J, PLOTKIN A, "Low Speed Aerodynamics", 2nd edition, Cambridge Press, 2001

KERWIN JE, "Marine Propellers", Ann. Rev. Fluid Mech., 18:367-403, 1986

LEE TJ, "A potential based method for the analysis of marine propellers in steady flow." PhD thesis, M.I.T. Dept. of Ocean Engineering, Aug 1987

MCMAHON J, "Characteristics of ducted propellers." SNAME Propeller/ Shafting Symposium 94, Paper 18.1-14, Virginia Beach USA, Sept 1994

MORINO L and KUO CC, "Subsonic Potential aerodynamics for complex configurations: A general theory." AIAA Journal, Vol.12, No.2, pp 191–197, Feb 1974

NEWMAN JN, "Distribution of sources and normal dipoles over a quadrilateral panel." Journal of Engineering Mathematics, Vol.20, pp113-126, 1986

PASHIAS C, "Shape Optimisation for a Long Range Autonomous Underwater Vehicle Using Computational Fluid Dynamics", BEng. Project, University of Southampton, 2001

PASHIAS C, TURNOCK SR, ABU-SHARK S, "Design optimisation of a bi-directional integrated thruster", SNAME Propeller/Shafting Symposium 03, Virginia Beach USA, Sept 2003

PEREIRA F, SALVATORE F, DI FELICE F and ELEFANTE M, "Experimental and numerical investigation of the cavitation pattern on a marine propeller." 24th Symposium on Naval Hydrodynamics, Fukuoka, Japan, July 2002

RYCROFT NC, TURNOCK SR,*"Three dimensional multiblock grid generation: Fleximesh"*, Ship Science Report 101, University of Southampton, November 1997

TURNOCK SR, MOLLAND AF and WELLICOME JF, "Interaction velocity field method for predicting ship rudder-propeller interaction." SNAME Propeller/Shafting Symposium 94, Paper 18.1-14, Virginia Beach USA, Sept 1994

TURNOCK SR and WRIGHT AM, "Directly coupled fluid structural model of a ship rudder behind a propeller." Marine Structures 13:53-72, Elsevier 2000

TURNOCK SR, "Technical manual and user guide for the surface panel code: Palisupan." University of Southampton, Ship Science Report No.100, Oct 1997

9 Appendix A

9.1 How to define a Propeller shape from a standard marine propeller table

This technical note explains the geometry of marine propeller and how to define the shape from a standard marine propeller table using a step-by-step guide.

Nomenclature

x_s, y_s	Section co-ordinates	[m]
x_{max}	Position of maximum thickness of section	[%]
x_{perc},y_{perc}	Section offsets from table	[%]
P	Pitch of the section at the required radius	[m]
D	Propeller diameter	[m]
R	D/2	[m]
ψ	Helix angle	[radians]
ϕ	Pitch angle of section	[radians]
r	Radius of section	[m]
x, y, z	Co-ordinates of propeller surface	[m]
c	Section chord length	[m]

9.2 Introduction

To define the propeller blade geometry the following system is used. The blade is formed starting with a midchord line defined by the radial distribution of skew angle $\theta_m(r)$ and rake $x_m(r)$. For the Subsea propeller both skew and rake are zero since it is symmetric. By advancing a distance $\pm$½ $c(r)$ along a helix of pitch angle $\phi_p(r)$, the blade leading edge and trailing edge are obtained. The surface formed by the helical lines is use as the reference upon which the sections can be built. These sections are defined in standard aerofoil terms by a chordwise distribution of camber $f(s)$ and thickness $t(s)$, where s is a curvilinear coordinate along the helix.

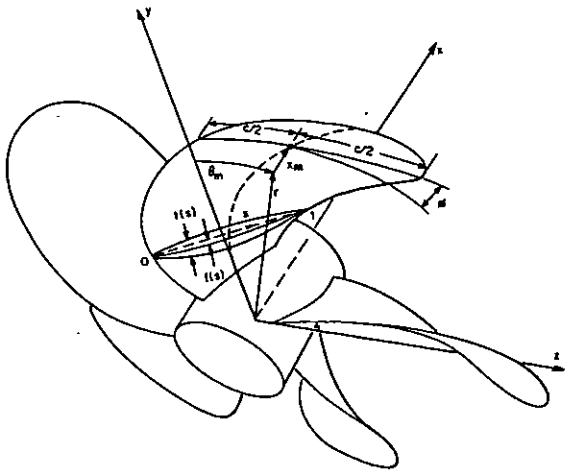

The helix is defined by the pitch angle, which is shown below. It is a function of pitch and radius.

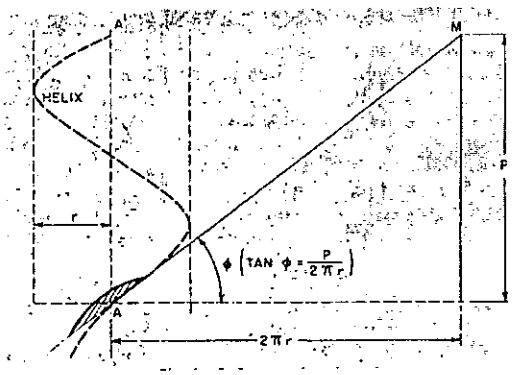

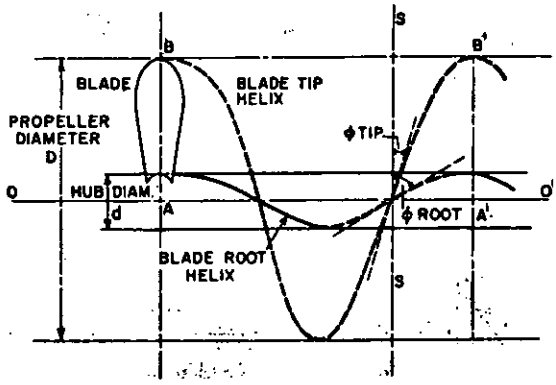

9.3 Standard propeller table

A marine propeller table contains information that defines the basic propeller geometry. The pitch, thickness, skew, rake and chord distribution of the propeller are defined in the table. To allow scalability of the propeller the information is non-dimensionalised usually with respect to the diameter of the propeller. The radial location of a section is non-dimensionalised by the overall radius R. The chord with respect to diameter. Skew and Rake are usually defined angularly. The thickness of the section is non-dimensionalised with respect to the local chord.

Ka-470 Propeller
section=9
diameter=0.3

r/R	c/D	Skew	Rake	P/D	t/c
0.2	0.231	0.0012	0	1	0.173
0.3	0.264	0.007	0	1.1	0.133
0.4	0.2935	0.004	0	1.15	0.102
0.5	0.32	0.002	0	1.2	0.077
0.6	0.345	0.003	0	1.25	0.055
0.7	0.365	0	0	1.3	0.038
0.8	0.379	0	0	1.3	0.024
0.9	0.388	0	0	1.3	0.016
1	0.389	0	0	1.3	0.013

Sample propeller table for Kaplan470

9.4 Standard section offsets

Propeller sections are usually expressed in two parts. From the trailing edge to the position of maximum thickness and from the maximum thickness to the leading edge. Offsets are given for the back and face in percentage form.

back

r/R	100	98	97	95	90	80	60	40	20
0.2	24	26	28	34	41	55	77.19	90.83	97.92
0.3	20.45	24	25.5	29.55	37.87	53.02	75.62	90.06	97.63
0.4	13.47	19	20	25.83	34.72	50	73.61	88.89	97.22
0.5	7.81	15	17	22.24	30.22	45.84	70.46	87.1	96.77
0.6	1	10	13	19	28.59	43.58	68.26	85.89	96.47
0.7	1	10	15	20	30.79	45.31	69.24	86.33	96.58
0.8	0.5	15	17	24	34.39	48.16	70.84	87.04	96.76
0.9	0.1	16.5	20	28	38.87	51.75	72.94	88.09	97.17
1	0.1	17	23	30	39.25	52	73	88	97

Section table for the back from trailing edge the maximum thickness.
There are another 3 tables for the other parts of the section.

To generate the x_s, y_s co-ordinates the standard table has to be transformed as follows:

For the trailing part of the section both for the face and back

$$x = x_{percent}(1 - x_{max}/100)$$

$$y = y_{percent}$$

For the leading part of the section both for the face and back

$$x = x_{percent}(x_{max}/100)$$

$$y = y_{percent}$$

The above results in a section with a chord and thickness of 100 with the position of maximum thickness at x=0. Then the section has to be scaled as detailed below. Care should be taken since offsets vary with different institutions.

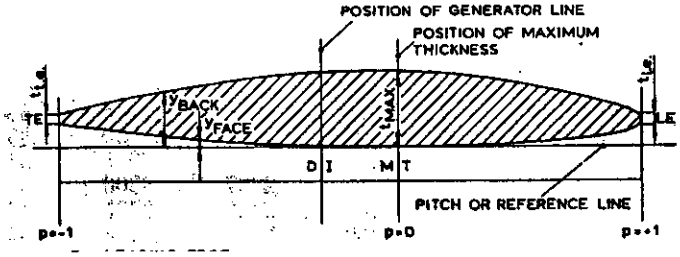

9.5 Step by step

1. Scale the 2D section to the required chord and thickness.
2. Make sure the mid-chord of the section is at x_s=0
3. Find the pitch angle ϕ using the following equation

$$\phi = \tan^{-1}\left(\frac{P}{2\pi r}\right)$$

1. Take x_s for the first point and using the equation below for the distance along a helix find angle ψ.

$$\psi = \frac{x_s}{\sqrt{r^2 + (P/2\pi)^2}}$$

2. Having found ψ we now know the position of that point on the helix. We can now map the section thickness by using the transformation matrix below.

$$\begin{bmatrix} x \\ y \\ z \end{bmatrix} = \begin{bmatrix} r\cos\left(\psi - \frac{y_s}{r}\sin\phi\right) \\ \frac{P\psi}{2\pi} + y_s\cos\phi \\ -r\sin\left(\psi - \frac{y_s}{r}\sin\phi\right) \end{bmatrix}$$

3. Go back to step 4 and repeat for all the points in that section
4. Go back to step 1 and repeat for all sections

9.6 Sample calculation

1. Scale the section to the correct c and t. From the propeller table the chord for the first section at (0.2*r) is 0.231*D since chord is non-dimensionalised with respect to D. There for chord=0.0693m. The thickness ratio is 0.173 of the chord, which is 0.012m. Scale the section to the correct chord and thickness.
2. Move the section such that the mid chord is at x=0, i.e. the trailing and leading edge should be at ±0.347m.

3. The propeller table gives pitch as non-dimensional P/D ratio. Multiply the value from the table by the diameter to get the pitch which is 0.3m for the first section. Then find the pitch angle ϕ which equals 1.01 radians.

4. Take x for the first point which is 0.347m and find ψ:

$$\psi = \frac{0.347}{\sqrt{(0.2*0.15)^2 + (0.3/2\pi)^2}} = 10.9rad$$

5. Find the x, y, z co-ordinates of the blade. The thickness for the first point is zero therefore y_s=0.

$$\begin{bmatrix} x \\ y \\ z \end{bmatrix} = \begin{bmatrix} 0.03\cos\left(10.9 - \frac{0.0}{0.3}\sin(1.01)\right) \\ \frac{0.3*10.9}{2\pi} + 0.0\cos(1.01) \\ -0.03\sin\left(10.9 - \frac{0.0}{0.03}\sin(1.01)\right) \end{bmatrix}$$

9.7 References

Kerwin JE, "Marine Propellers", Ann. Rev. Fluid Mech., 18:367-403, 1986

Turnock, S.R., *"Prediction of ship rudder-propeller interaction using parallel computations and wind tunnel measurements"*, University of Southampton, PhD Thesis, 1993

Lewis, "Principles of naval architecture: VolumeII: Resistance, propulsion and vibration", SNAME, 1988

10 Appendix B

10.1 User guide to propgen

This is a brief description of the important variable used to define the propeller geometry within propgen.

10.2 Propeller table

In order to define the propeller a table format is used. The first line contains the name or a description of the propeller. This is followed by the number of sections used to define the propeller. They are like control points on the surface where the chord, pitch, skew, rake and section shape are defined. Next is the overall diameter of the propeller. The values in the table are non-dimensionalised with respect to this to enable easy scaling. Finally the table defining the propeller is defined. The first section is located on the hub. The radial location is defined as the non-dimensional distance from the shaft axis to the blade tip. The chord is non-dimensionalised with respect to diameter. Skew and rake are angular measurements and do not need to be non-dimensionalised. The pitch diameter ratio is followed by the thickness which is non-dimensionalised with respect to the chord length at that section.

DMTB P4119
sections= 10
diameter= 0.3048

Radius	Chord	Skew	Rake	P/D	Thickness
0.2	0.32	0	0	1.105	0.2055
0.3	0.3625	0	0	1.102	0.1553
0.4	0.4048	0	0	1.098	0.118
0.5	0.4392	0	0	1.093	0.0916
0.6	0.461	0	0	1.088	0.0696
0.7	0.4622	0	0	1.084	0.05418
0.8	0.4347	0	0	1.081	0.04206
0.9	0.3613	0	0	1.079	0.03321
0.95	0.2775	0	0	1.077	0.03228
0.98	0.03	0	0	1.075	0.0316

Propeller table for the DTMB4119 propeller

10.3 Section definition

Accompanying the propeller table is file containing a section list. This section list defined the files and paths of the sections referenced in the propeller table. It contains the same number of sections as defined in the propeller table followed by the duct section and cap section. The sections can be different for each location or the same. Each section file contains the number of points for the section followed by the points' x and y coordinates.

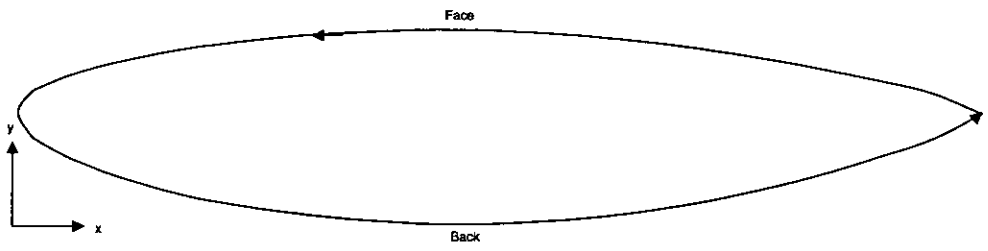

Correct definition of sections

The sections' coordinates must be defined in a specific manner in order to ensure that later on when the mesh is created the panels point outward and not inwards causing problems.

10.4 Propoptions file

The last file required is the propoptions file. It contains several parameters which control the propeller generation process. Comment lines can be added to the propoptions files if they are preceded by an exclamation mark. There are five groups of variables: blade, hub, duct, cap and ring. They define variables concerning each part of the geometry. The name of the variable contains the part of the geometry it controls followed by the faction. A summary follows:

10.5 Blade variables

blade_number=3	Number of blades
blade_advance_speed=3.0	Advance speed in m/s
blade_rps=20	Revolutions per second of the propeller
blade_ns=21	The number of nodes in the chordwise direction for the blade
blade_nt=4	The number of nodes between sections
blade_wake_length=3	The length of the blade wakesheet in diameters
blade_wake_free_length=0.333	The ratio of the free wakesheet length to the overall wakesheet length
blade_wake_fixed=160	The number of nodes on the fixed wake
blade_wake_free=80	The number of nodes on the free wake
blade_P=0.3 blade_Q=1.0	Parameter controlling the chordwise clustering of the panels
blade_tip_cluster=1	Increase the number of spanwise nodes by this factor for the slice near the tip
blade_wake_contraction=0	0 neglects wake contraction 1 takes into account wake contraction Can take values in between 0 and 1
blade_wake_transition=1	The distance in diameters the pitch of the wake transitions from the blade pitch to the final pitch
blade_wake_final_pitch=0.8	Defines the final wake pitch. If negative the pitch is calculated within the program

10.6 Hub Variables

Hub_length=0.08	The length of the hub in diameters
Hub_nt=8	The number of radial nodes for each hub strip
Hub_ns=4	The number of nodes for the leading and trailing

	part of the hub
Hub_strips=3	The number of hub strips. Possible values 3, 4, 5, 6 and 8. Default is 3
Hub_vleading=0.3 Hub_vtrailing=0.3	Controls the hub v angle. Values between 0 and 1.
Hub_offset_le=0	Shifts where the hub edge attaches to the root section to avoid problems with the hub mesh near the blade root

10.7 Cap variables

Cap_section_auto=1	1 generates hemi-spherical cap 0 reads cap section from file
Cap_side_length=0.9	The non-dimensional distance along the cap edge where the V attaches to the side
Cap_internal lenth=0.8	The non-dimensional distance along the cap middle where the point of the V is located. Has to be more than the cap_side_length
Cap_nt=14 Cap_ns=14	The number of nodes on the hub edges

10.8 Duct variables

Duct_length=0.8	The duct length in diameters
Duct_thickness=0.166	The thickness of the duct as a percentage of length
Duct_images=4	The number of duct images
Duct_wake_length=6	The wake length in duct lengths
Duct_wake_free_length=0.333	The ratio of the free wakesheet length to the overall wakesheet length
duct_wake_free_ns=30 duct_wake_fixed_ns=30	The nodes for the wake (see blade)
duct_P=0.3 duct_Q=1.0	Control the clustering of the panels on the duct
duct_nt=3	The number of nodes between each section of the duct (10 in total)
duct_upper_ns=25 duct_leading_lower_ns=7 duct_trailing_lower_ns=7	The number of nodes in the chordwise direction on the duct

10.9 Example propoptions file

```
!Duct options
!use lower case
duct_length=0.8
duct_thickness=0.1667
duct_nt=3
duct_upper_ns=25
duct_leading_lower_ns=7
duct_trailing_lower_ns=7
duct_wake_free_ns=30
duct_wake_fixed_ns=30
duct_wake_length=6
duct_wake_free_length=.33
duct_images=3
duct_P=0.3
duct_Q=1.0

!Blade options
blade_number=3
blade_nt=3
blade_ns=20
blade_wake_length=3
blade_wake_free_length=.33333
blade_wake_fixed_ns=160
blade_wake_free_ns=70
blade_P=1.0
blade_Q=0.1
blade_advance_speed=0.6
blade_rps=20
blade_tip_cluster=1
blade_wake_contraction=0
! diameter lengths
blade_wake_transition=1
!if final wake pitch is negative or zero it
!is calculated within the program
blade_wake_final_pitch=-0.8

!Ring options
!for no ring put ring_width =0
!ring_width is the gap in the ring as a % of prop D
ring_width=0
ring_split=1
ring_nt=10
ring_strips=2


!Hub options
!strips possible values 3 4 5 6 8 default 3
hub_strips=4
```

```
hub_nt = 8
hub_ns = 4
hub_length=0.09
hub_vtrailing=0.3
hub_vleading=0.5
!moves the point on the leading edge of the blade where the hub starts
!default is zero but for very thick blade noses use 1
hub_offset_le=0

!Cap options
!internal_length has to be less than cap_side_length
cap_internal_length=0.9
cap_side_length=0.95
cap_nt=5
cap_ns=13
!set to 1 to generate spherical cap automatically
!set to 0 to read from a file defined in section_list
cap_section_auto=0
```